Microgravity measurement of the Soret effect in a molten salts mixture

1997 J. Phys.: Condens. Matter 9 11045

(http://iopscience.iop.org/0953-8984/9/50/010)

J. Phys.: Condens. Matter **9** (1997) 11045–11060. Printed in the UK PII: S0953-8984(97)79626-7

Microgravity measurement of the Soret effect in a molten salts mixture

J Bert and J Dupuy-Philon

Université Claude Bernard—Lyon I, Département de Physique des Matériaux (CNRS-UMR 5586), Lyon-Villeurbanne, France

Received 18 November 1996, in final form 6 October 1997

Abstract. We have performed the first measurement of the Soret effect in a molten salt mixture under microgravity conditions during two different flights (D1 and D2) of the spacelab. After justifying our selection of the molten salt used (AgI/KI) and a description of the microgravity facility, we give the results of a three-dimensional simulation of combined convection phenomena and thermal diffusion effects. This simulation verifies the feasibility of the experiment and aids selection of the various geometric and physical parameters of the experiment.

The Soret coefficient deduced from these measurements is positive, corresponding to a heavy component migrating towards the cold end of the cell. Its value deduced from the thermopower is slightly different for the two flights (1.0×10^{-3} K^{-1} for D1 and 0.7–0.9×10^{-3} K^{-1} for D2) while the salt analysis after return to Earth gives the value 1.4×10^{-3} K^{-1} but for an experiment duration corresponding to about one time constant. Its is concluded that useful measurements of thermodiffusion are really possible in good conditions in space, but blind measurements must necessarily be confirmed by optical measurements in order to demonstrate the possible convection of the liquid and to know the real level of separation attained, compared with the perfectly nonconvective situation.

1. Introduction

The application of a thermal force to a fluid mixture induces a transport of matter which is coupled to the thermal field. This phenomenon, called the Soret effect [1–4], is not well understood for both theoretical and experimental reasons: theoretically because understanding of the heat of transport is still poor and experimentally because liquids which generally have a low viscosity are very sensitive to gravity induced instabilities which are bound to the direction of the mass transport.

Molten salt mixtures are thus highly affected by this problem, having a gravity-induced Rayleigh number around 100 per degree of temperature difference (50 times higher than for a liquid metal) for a cell aspect ratio (length/radius) of about 10. Despite this, they are interesting fluids for thermal-transport studies because of their relatively well known equilibrium and transport properties over the entire concentration range [5]. In addition, the total potential energy can be assumed to be pairwise additive and structure and transport properties can be calculated by molecular dynamics. Also, molten salts are transparent media in the visible spectrum and good ionic conductors, thus allowing diffusion measurements by means of an electromotive-force variation and/or optical methods.

The space shuttle gives microgravity levels of around $10^{-3}g_0$ or lower, g_0 being the Earth's gravity, which permits us to obtain Rayleigh numbers smaller than the critical value in the same confinement conditions (same aspect ratio). It seemed interesting to use this

0953-8984/97/5011045+16$19.50

experimental facility during a long-duration experiment in order to obtain direct experimental evidence of thermal diffusion in a molten salt mixture.

Numerous experimental problems have had to be mastered in order to perform this experiment in conditions of complete confinement without any free volume. Indeed, the melting positive volume expansion is difficult to estimate quantitatively. It was necessary to use a controlled porosity cell wall to absorb this expansion, without allowing the fluid to get into the pores by a simple capillary effect. The necessary use of controlled and stable temperature gradients during long times (more than 20 h) has been a real experimental problem, again reinforced in the space environment. At last, the choice of various aspect ratios insuring the hydrodynamical stability have led to a preliminary theoretical study.

In this paper, we present the results of three experiments performed during two space flights. We first discuss the suitability of the selected mixtures, then the original set-up designed for the accomodation of the volume expansion when melting; we then justify the choice of cell aspect ratio on the basis of a mechanical-stability study. In section 3, we discuss the experimental data. Finally, we propose an experiment making it possible to visualize and analyse successively an interdiffusion process, a thermal diffusion process and the triggering of instabilities on Earth and in space.

2. Selected mixture and important parameters

The phase diagram of the selected mixture, AgI_xKI_{1-x}, x being the mole fraction in silver iodide, is shown figure 1. This diagram, which was redetermined at our request by Claudy *et al* [6], differs substantially from that reported previously [7]. Two defined compounds KAg_4I_5 and K_2AgI_3 are formed and a deep eutectic at 238 °C is obtained for the composition $AgI_{0.72}KI_{0.28}$. The melting points of the pure compounds remain at 552 °C for AgI and 685 °C for KI. A peritectic line at 258 °C is present on the AgI side of the diagram.

Molar volumes measured by neutron-transmission attenuation [6] show a small positive deviation from regular behaviour. The thermodynamic excess functions can also be obtained by calorimetry and activity determination [8]; these last data are also important for the derivation of the interdiffusion coefficient from experimental measurements [4].

Because interdiffusion coefficients are known only in dilute AgI/KI mixtures [5], we tried to estimate D_{Ag^+/K^+} using an indirect method from individual self-diffusion and the Darken equation. We first measured the self-diffusion coefficients of the two cations Ag^+ and K^+ [9] with a capillary method and radioactive tracers, first introduced by Anderson and Saddington [10] for aqueous solutions then adapted for molten salts. The measured self-diffusion values (reproduced from [9]) are given in table 1; they correspond to two very low concentrations on both sides of the phase diagram and to a concentration close to the eutectic composition. We did not choose the exact eutectic composition because at the time these experiments were performed, the actual phase diagram was unknown. Then, by considering the nearly regular behaviour of the excess volumes, the Darken equation [9] makes it possible to estimate the interdiffusion coefficient using figure 2 to derive the thermodynamic factor Γ:

$$D_{Ag^+/K^+} = \Gamma[x_{Ag^+}D_{K^+} + x_{K^+}D_{Ag^+}] \tag{1}$$

with

$$\Gamma = 1 + \frac{\partial \log \gamma}{\partial \log x} = 1 + 1.07 = 2.07 \qquad \text{(around eutectic)}. \tag{2}$$

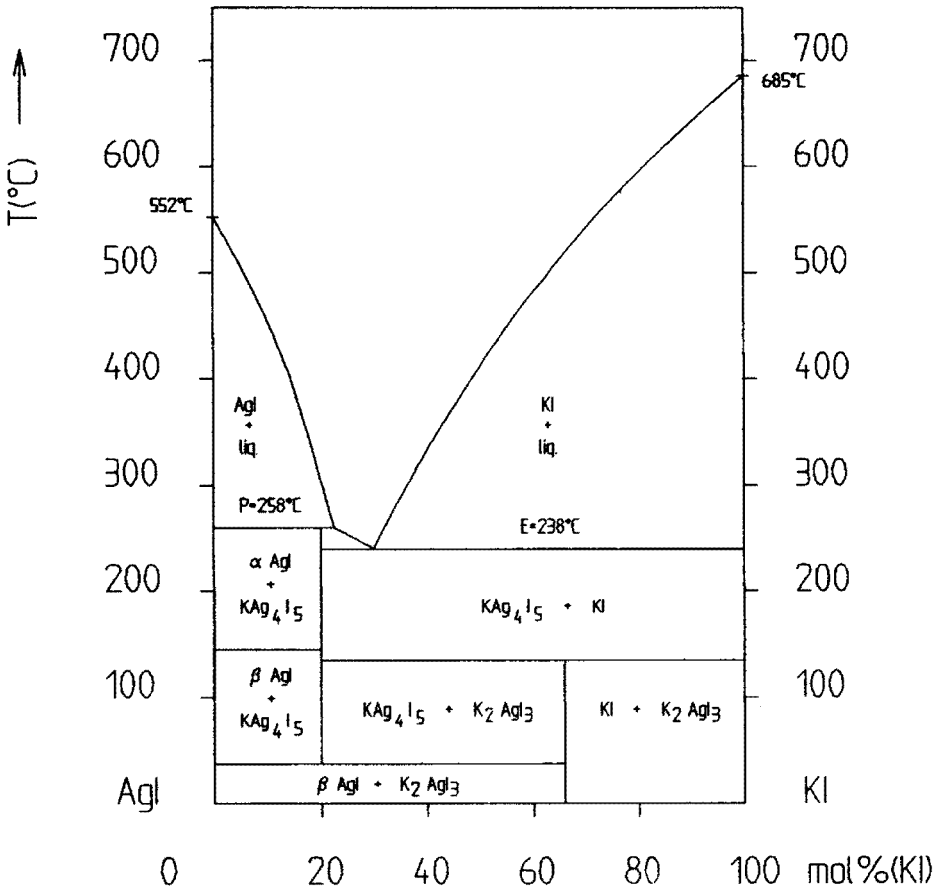

Figure 1. Phase diagram of AgI_xKI_{1-x} according [6] (x is the mole fraction of silver iodide).

Table 1. Ag^+ and K^+ self-diffusion coefficients in AgI_xKI_{1-x} according to [9].

KI % mole fraction in AgI_xKI_{1-x}	Temperature (°C)	Ion	Self-diffusion coefficient (10^{-5} cm^2 s^{-1})	Standard deviation (10^{-5} cm^2 s^{-1})
0	615	Ag^+	7.55	0.17
1.5	735	K^+	6.86	0.13
1.5	735	Ag^+	9.85	0.60
25	365	K^+	14.27	2.09
25	365	Ag^+	13.23	1.47
25	735	K^+	16.89	3.35
25	735	Ag^+	19.70	3.35
95	735	Ag^+	6.25	0.26

Equation (1), called the quasi-Darken equation is analogous to the Darken equation valid for a binary mixture of molten salts having a common anion, when the partial molar volumes are constant.

Finally, see figure 3, we give the interdiffusion coefficient measured at constant

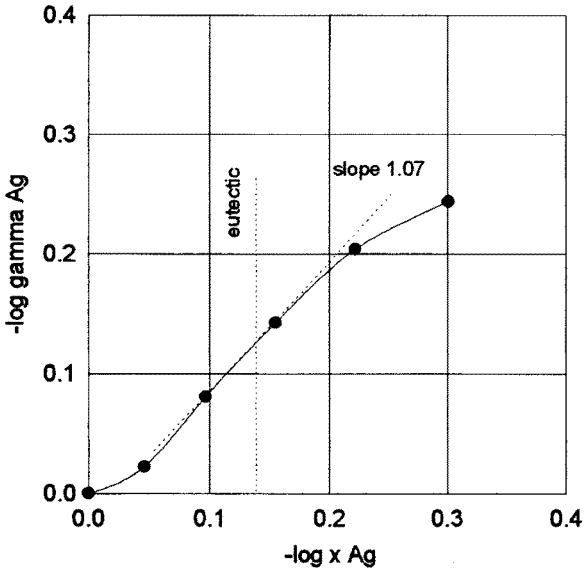

Figure 2. Activity factor measured by Sternberg [8].

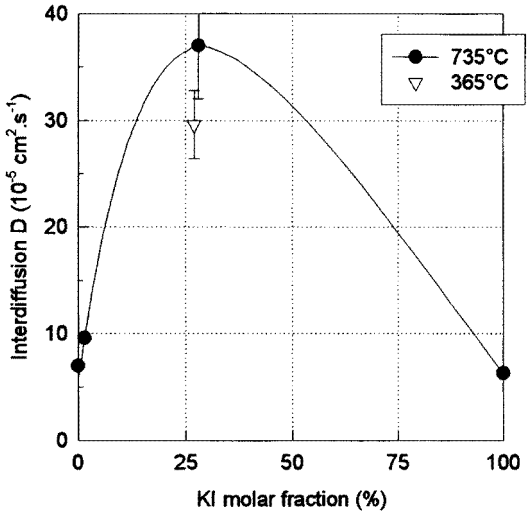

Figure 3. Interdiffusion coefficient calculated with the Darken equation using the measured self-diffusion coefficients.

temperature. Around the eutectic composition one gets a sharp increase of this coefficient compared with the dilute concentration values for which our data are similar to that of the literature. However, this increase is reduced if one considers equivalent temperatures T, defined by a constant ratio T/T_{liquidus}. The eutectic interdiffusion D_{Ag^+/K^+} evaluated from the individual motions of ions is then 37×10^{-5} cm^2 s^{-1}. The sharp maximum shows the interest of measurements around the eutectic temperature, especially when the expected effect is small, which is the case of the Soret effect.

According to Tyrrell [4], the 'characteristic time' or time constant of the mass transport

is bound to the interdiffusion coefficient and also to the length h of the diffusion cell by the formula,

$$\tau = \frac{h^2}{\pi^2 D_{Ag^+/K^+}}. \tag{3}$$

For example, if h is equal to 3 cm, τ is about 0.75 h at the eutectic composition.

3. Experimental set-up

3.1. Furnace

All experiments were performed in the French space agency (CNES) gradient heating facility (GHF). This furnace was developed by the CNES for the first spacelab mission payload (FSLP) in 1983. After this successful flight, it was again used for D1 in 1985 and finally, for D2 in 1993. This furnace is able to hold a set of three experimental cartridges C1, C2, C3 each having three heating zones. This allows the possibility of setting a high- and low-temperature zone for each cartridge, the longitudinal temperature gradient being generated by three heating zones called heater and transmitted to the cartridges by diffusors. A heat sink permits us to transfer the heat outside the cartridges [11–15]. An adequate heating programme combined with carefully calculated thermal design of the inner part of each cartridge makes it possible to perform two or three different experiments during each run.

3.2. Thermodiffusion cell

3.2.1. Description. The thermodiffusion cell satisfies five design criteria:

- chemical inertia and tightness at all temperatures;
- total filling (100%) to avoid surface effects;
- electrical integration of silver electrodes for thermoelectric measurements (potential difference generated by the temperature gradient along the cell axis);
- highest possible temperature gradient;
- flight security.

A cell satisfying these requirements is shown figure 4. The main part takes the form of two pure alumina concentric cylinders (1) and (2). The external one (1) has a zero porosity whereas the internal one (2) has a porosity of 18% volume (pore diameter 30 μm). The adjustment tolerance of the two cylinders is $\frac{1}{100}$ mm. The salt fills the total inner cylinder (length 30 mm, radius 2.5 mm—aspect ratio 12—or radius 1.5 mm—aspect ratio 20). The

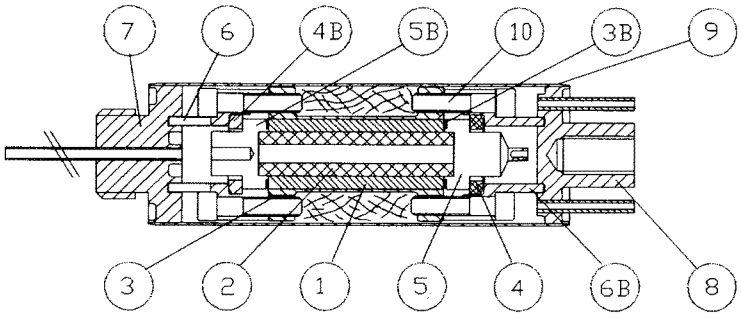

Figure 4. Thermodiffusion cell. The description is given in the text.

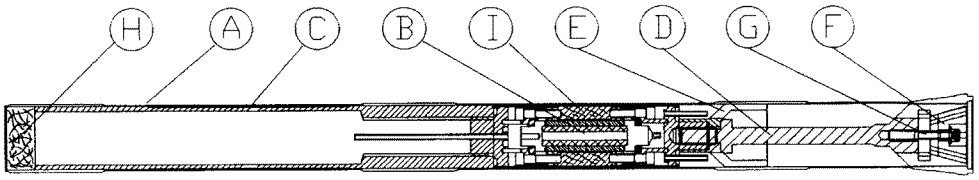

Figure 5. Thermodiffusion cell inside the GHF cartridge. A-Pyrad 49 D cartridge, B-thermodiffusion cell, C-copper or stainless steel for hot end, D-copper or nickel for cold end, E-thermal coupling copper piece, F-copper cone for thermal coupling, G-stainless steel screw for copper cone, H-carbon fibre for compensation of thermal expansion, I-zirconium oxide fibre (thermal screening).

thermodiffusion cell is closed by silver plugs (5 and 5B) which act as electrodes for the thermopotential measurements. Impervious closure is ensured by silver o'rings. Closure of the alumina external tube is effected by means of a non-expanding metal tube (3) and stainless steel plugs (6) and (6B), tightened with screws. The alumina tube (1) is optically polished on both ends to ensure perfect closure. One end (5) (cold end) is electrically insulated by an alumina ring (4), the other one (5B) (hot end) being connected to the frame. The cell, its electrodes and its thermocouples are placed in a stainless steel tube (9) which ensures the protection in case of accidental breakage of the alumina tube. The plugs (7) and (8) are soldered to the tube (9) by electronic bombardment as are the thermocouples and electrodes wires (not shown). The heat flux and the thermal exchange are improved by an atmosphere of about 1000 Pa helium inside the protection tube together with the whole GHF cartridge which design is given figure 5.

3.2.2. Cell filling. As already noted, it is essential for the cell to be completly filled in order to avoid surface convection (Marangoni effect). For this purpose, the mechanical fittings were carefully executed. In addition, the alumina porosity (30 μm) was chosen in order to absorb the expansion completely during the melting, i.e. under the influence of the resulting pressure and not by a simple capillary effect. Total filling is also necessary to maintain the electrical contacts between the two electrodes. The efficiency of the porous alumina was visualized by neutronography because the neutron absorption of the salt ($\mu = 0.813$ cm^{-1}) which is much higher than that of porous alumina ($\mu = 0.4$ cm^{-1}), enables the detection of the salt in the pores which produces a contrast modification. This method also permits the control of a good tightness as well as the contact quality and stability which can be visualized under the neutron beam during the thermoelectric measurements.

3.2.3. Thermal performances. Apart from a few minor modifications, the same set-up was used for D1 and D2 flights. In both cases the temperature rise time was about 0.75 h for the fusion of the samples, then a further 0.25 h was required for an approximately stable gradient and 0.25 h more for a good stable gradient (the temperature gradient is said to be stable when it approaches its terminal value—30–75 °C cm^{-1}—with a difference smaller than 2 °C cm^{-1}).

A minimum time between the fusion of the sample and the establishment of a stable gradient ensures a reasonable knowledge of time zero for diffusion which is determined through the measured thermoelectric potential. This precise instant takes place when the gross variations coming from the establishment of the temperature gradient are completed. The resulting uncertainty is about 15 min, consistent with the durations of the experiments.

Table 2. Experimental conditions during both flights and for the three cartridges of the GHF furnace (temperature approximated)—the measurements discussed in this paper—D1 experiment 2–C1 and D2–C1 are in bold type.

Flight	Side	C1	C2	C3
D1	Cold	380 °C	380 °C	380 °C
experiment 1	Hot	600 °C	600 °C	600 °C
5 h ΔT	composition	$AgI_{0.72}KI_{0.28}$	$AgI_{0.72}KI_{0.28}$	$AgI_{0.72}KI_{0.28}$
	aspect ratio	20	20	12
D1	Cold	**380 °C**	380 °C	380 °C
experiment 2	Hot	**600 °C**	600 °C	600 °C
5 h ΔT	composition	$\mathbf{AgI_{0.72}KI_{0.28}}$	$AgI_{0.72}KI_{0.28}$	$AgI_{0.72}KI_{0.28}$
	aspect ratio	**12**	12	20
D2	Cold	**410 °C**	410 °C	325 °C
	Hot	**510 °C**	510 °C	440 °C
24 h ΔT	composition	$\mathbf{AgI_{0.80}KI_{0.20}}$	$AgI_{0.72}KI_{0.28}$	$AgI_{0.72}KI_{0.28}$
	aspect ratio	**20**	20	20

For D2, accounting for our gained experience, the thermal performance was slightly better than for D1.

In D1, the real magnitude of the Soret effect being unknown, an attempt was made to maximize the applied temperature gradient. In D2, as we roughly knew the Soret coefficient value (absolute value and sign), the temperature and the gradient were slightly reduced. In addition, after careful thermal calculations and Earth calibrations, we managed to obtain two different thermal conditions for the three cartridges. In D1, the three cartridges had the same composition (eutectic) while in D2, we had two different compositions of the melt with matching temperatures. The various experimental conditions are summarized in table 2 [16].

4. Hydrodynamical stability criteria

4.1. Description of the performed simulation

Thermal diffusion is a very slow process, so if a global fluid motion appears in the cell, a more or less important perturbation of the measurements can occur. In order to quantify the convective motions and to suitably determine the cell dimensions, we made a complete theoretical analysis of the mechanical phenomena before the space experiment. We first considered [11, 16] the case of vertical geometries with the temperature gradient parallel to gravity and performed a linear stability study. This led us to introduce the notion of an instability threshold which separates a domain of rest from a domain with convective motions and hence to show that, in low gravity conditions, a good choice for the aspect ratio might systematically put the system in a stable situation. In a spatial experiment the cell orientation with respect to the residual gravity, including the g-gitters, cannot be controlled. It is therefore necessary to deal with other situations for which convection cannot be avoided in order to see how it influences the separation phenomenon. We realized a direct simulation of three-dimensional convection in a cylinder taking account of thermal diffusion. The results show that instead of an instability threshold, we should rather speak of a threshold corresponding to situations for which the convective motions alter, in a sensitive

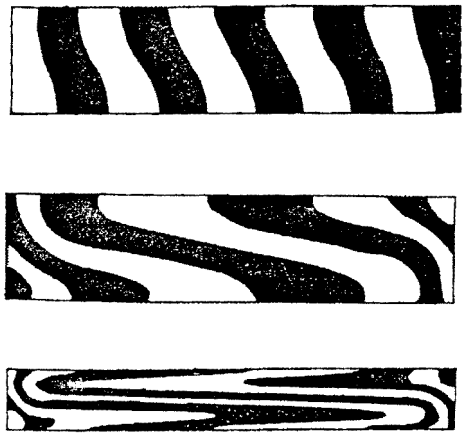

Figure 6. Theoretical mass fraction profiles in various microgravity situations. Top: $g = 10^{-4}g_0$, $Ra = 0.434$ (aspect ratio 6); centre: $g = 10^{-3}g_0$, $Ra = 4.34$ (aspect ratio 6); bottom: $g = 10^{-1}g_0$, $Ra = 660$ (aspect ratio 10).

manner, the mass-fraction profiles created by the thermal diffusion.

The mathematical simulation has been performed with a finite-difference method for reduced-gravity situations, when the cell is horizontal, i.e. with its axis perpendicular to the residual gravity forces, which is the worst case for convection. The lateral walls are assumed to be conducting compared with the salt (the ratio of the related thermal conductivities being about 15). The calculations have been performed with the numerical values corresponding to that of the molten $AgI_{0.72}KI_{0.28}$ mixture. The dimensionless Prandtl and Schmidt numbers were then respectively $Pr = 0.6$ and $Sc = 60$. The theoretical temperature gradient was $100\,^{\circ}\mathrm{C\ cm^{-1}}$ which corresponds to Rayleigh number values of 4.34 and 0.434 for respective gravity values of $10^{-3}g_0$ and $10^{-4}g_0$, g_0 being the Earth's gravity. The cell aspect ratio (length/radius) was either 6 or 10.

4.2. Main simulation results

First, the temperature profiles are perfectly linear for both gravity levels. Second, the mass-fraction profiles (figure 6) show that the iso-mass-fraction curves are more or less tilted by the motions. This means that the thermally induced separation is perturbed and does not automatically attain its maximum value corresponding to the perfect Soret effect (absence of convection).

Let us normalize these results and give the arbitrary value 1 to the perfect separation (without convection), then the separation will be 0.98 for $10^{-4}g_0$ and 0.46 for $10^{-3}g_0$. For stronger Rayleigh, the mass-fraction profile is much more perturbed and the separation becomes smaller than 0.30 (table 3). The calculated velocities are rather small in the first two cases (order 10^{-3} cm s^{-1}) and correspond to a good thermally conductive regime as the isotherms are not tilted by convection. In the third case, the velocities can be estimated between 0.1 and 1 cm s^{-1}; they correspond to a convective regime. The useful conclusion of this preliminary theoretical hydrodynamical study is that for gravity values lower than $10^{-4}g_0$, the separation is almost perfect; for gravities larger than $10^{-3}g_0$, the separation is undoubtedly perturbed by the flow, the perturbation increasing with the gravity level.

As the experimental microgravity levels were expected to be between $10^{-3}g_0$ and

Table 3. Summary of the obtained numerical results. Horizontal cylindrical cell containing eutectic AgI KI mixture. Aspect ratio (length/radius = 6; temperature gradient = 100 °C cm^{-1}; Prandtl $Pr = 0.6$; Schmidt $Sc = 60$.

Gravity level	$> 10^{-1} g_0$	$10^{-3} g_0$	$10^{-4} g_0$
Rayleigh Nr	> 434	4.34	0.434
Temperature profile	slightly perturbed	linear	linear
Iso-mass fraction profile	much perturbed	perturbed	slightly perturbed
Separation induced by thermodiffusion	0 to 0.30	0.46	0.98

$10^{-4} g_0$, we chose to increase the cell aspect ratio (values 12 and 20) in order to get a better confinement, so a better stability (table 2). The use of two different aspect ratios was made for D1 only, because we wanted to test a possible influence of this parameter on the thermodiffusion results.

5. The two space experiments

5.1. Description of the D1 experiment

The aim of the D1 experiment was to obtain the first space thermodiffusion values. The problem was complex for two reasons:

- first, Earth experiments and a few calculations had shown that the Soret coefficient is rather small [17, 20];
- second, the real direction of thermodiffusion relative to the temperature gradient was unknown, as was the direction of variation of the resulting thermoelectric power (increasing or decreasing). In other words, the sign of the Soret coefficient was unknown.

We therefore set out to maximize the thermal gradients in order to get the largest possible experimental and visible effects. This experiment was conducted with a gradient of 75 °C cm^{-1}, with a eutectic mixture which shows the largest interdiffusion coefficient (figure 3), and a duration of 5 h, roughly equal to six times the expected diffusion time constant. During D1, two runs were performed: one scheduled normally during the first part of the flight and the second using spare cartridges at the end of the flight. As many other experiments took place at the same time as the first experiment, we experienced temperature and vacuum instabilities. Better and more reliable results were obtained with the second experiment (when no other experiment was running at the same time). For this reason, we describe only the last experiment. Our aim was to make the first precise determination of the real Soret coefficient and compare our values with numerical calculations. Our simulation was designed to explore the theoretical convective stability of such systems and determine the best geometrical cell characteristics for the space experiment. We made an assumption about the mean microgravity value and the perturbations which could appear during the experiment, then considered two types of cell with different aspect ratios (12 and 20).

As a sufficient number of amplifier outputs was not available (space specifications are tight for energy consumption reasons), we could not measure the absolute temperature together with the temperature difference for each cell, so we chose to measure the temperature difference on C1 and C2 and the absolute temperature on C3. This appears not to have been the best choice because the thermal configuration asymmetry combined with unidentical furnace behaviours on Earth and in space, made it impossible to get the correct

temperature difference in the third cell (even by computation). We thus lost a large part of the results connected with this cell.

5.2. Description of the D2 experiment

As shown below, the thermodiffusion effect we obtained in D1 was measurable, but the time constant was much larger than expected, the aim of D2 was therefore slightly different from that for D1 [19]:

- first, the duration had to be increased significantly because the stationary state was far from being attained during the D1 5 h under gradient;
- second, the direction of the thermopower variation, as well as the order of magnitude of the diffusion coefficient, were known, so was it possible to work with smaller gradients (about $30\,^{\circ}\mathrm{C\ cm^{-1}}$ instead of $75\,^{\circ}\mathrm{C\ cm^{-1}}$);
- third, we were able to exploit the thermal possibilities offered by the GHF after the thermal calculations performed in CNES in Toulouse.

This procedure led us to propose a 24 h experiment under gradient with the possibility of undertaking three different experiments (see table 2).

On Earth, during the qualification experiment, the stability of both the temperature of the cold end of the cell and the gradient was good to within a few tenths of a degree over a 24 h period. In space, the absolute temperature was not measured because too few amplifier ouputs were available. The stability of the measured temperature differences was not better than plus or minus $2.5\,^{\circ}\mathrm{C}$ due to large instabilities of the furnace low-temperature zone ($\pm 5\,^{\circ}\mathrm{C}$ over a 24 h period). In D1, the temperature results were similar but only covered a 5 h period.

In D2, for the reason given above, we chose not to measure the absolute temperature, but only the temperature difference. The results were again perturbed, as for D1. In addition, we had experimental problems with two of our three cells arising from variation of the wetting properties of porous alumina with salt composition. Consequently only the C1 results sequence is available.

5.3. Thermopower results

The D1 and D2 thermopower experimental results (ratio of the potential difference to the temperature difference between the two electrodes) are shown in figure 7. For clarity, we have not plotted all the experimental points (one series of measurements every 4 s during the whole flight), but the calculations are performed with all the measurements values. The calculated curves also given in figure 7 will be discussed below.

The dominant point, visible on the lower curve (D1) is that diffusion is much slower than initially predicted: after 5 h of diffusion, the diffusion process was still very active. This means that the interdiffusion coefficient is much smaller than calculated after the Earth determination of the self-diffusion coefficients. In contrast to D1, the D2 duration is sufficient (upper curve), but it is evident that after 5 h, the results were perturbed during this experiment; this point will be discussed in the following.

Again, for clarity, in figure 7, we have chosen not to correct the values for additional metal contact potential differences which were important for D2; this explains the vertical shift between D1 and D2 (roughly $0.04\ \mathrm{mV\ ^{\circ}C^{-1}}$). However, as these stray contact potentials are constant during a whole experiment (at constant temperature), the results obtained (time constant, interdiffusion coefficient and Soret coefficient) are not affected by this shift.

The theoretical variations of the thermopower with time can be obtained by the

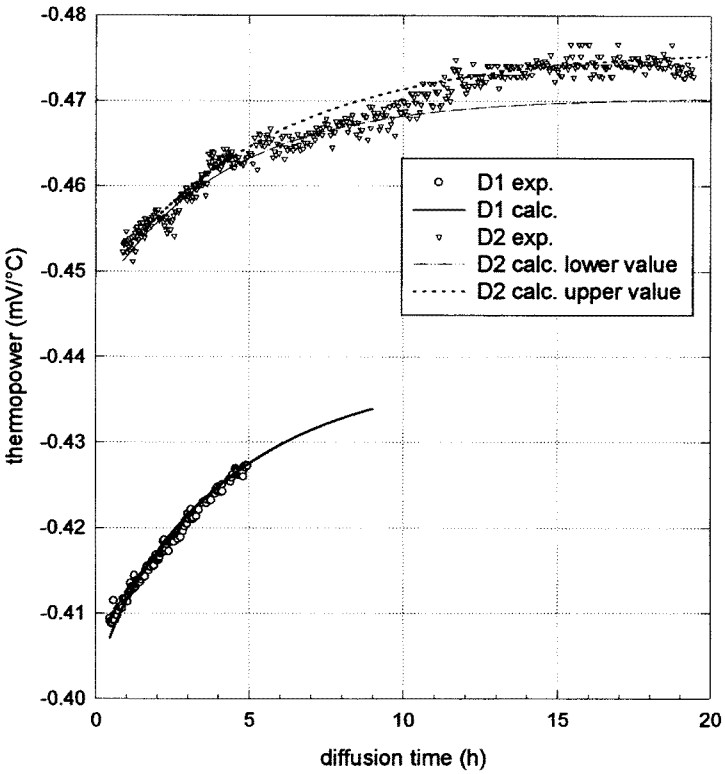

Figure 7. Thermopower results with time for D1–C1 experiment 1 (lower values) and for D2–C1 (upper values) and corresponding curve fits. For D2, due to the problems appearing during the flight, two calculated curves are given (explanations in the text).

integration of a simplified flow equation in which it is first assumed, that no convective flow occurs, second, that the vertical walls have no influence on the process and third that the temperature gradient is constant along the main direction. These assumptions, with the help of the phenomenological theory, lead to a modified Fick's second law which can be solved with approximations which are different for short times and for long times [4]. The expressions obtained for the thermopower are:

$$\varepsilon_t - \varepsilon_0 = (\varepsilon_\infty - \varepsilon_0)2\pi^{-3/2}(t/\tau)^{1/2}(1 - y_1) \qquad \text{for } t < \tau \tag{4}$$

$$\varepsilon_t - \varepsilon_0 = (\varepsilon_\infty - \varepsilon_0)[1 - 8/\pi^2 \exp(-t/\tau)] \qquad \text{for } t > \tau \tag{5}$$

with $y_1 = 2\pi^{1/2}\text{ierfc}[\pi/2(t/\tau)^{-1/2}]$, ierfc being the integral error complementary function.

In these expressions, ε_t, ε_0 and ε_∞ respectively represent the thermopower at time t, at time 0 and at infinite time; τ is again the time constant. Equation (5) is valid only for long times while equation (4) is only valid for short times. In the time domain $0.5\tau < t < 2\tau$ the two equations overlap with a relative error of about 10^{-3}. The term y_1 of equation (4) can be neglected for times smaller than 0.5τ. The complicated form of equation (4) shows that it is easier, to evaluate long-duration experiments, the advantage being that it is then possible to fit the results with a simple exponential equation and obtain both ε_∞ and the Soret coefficient S_T with greater precision.

In figure 8, we give the D2 fits, obtained with the two kinds of calculations (long times and short times). They show that the influence of the exponential terms becomes important

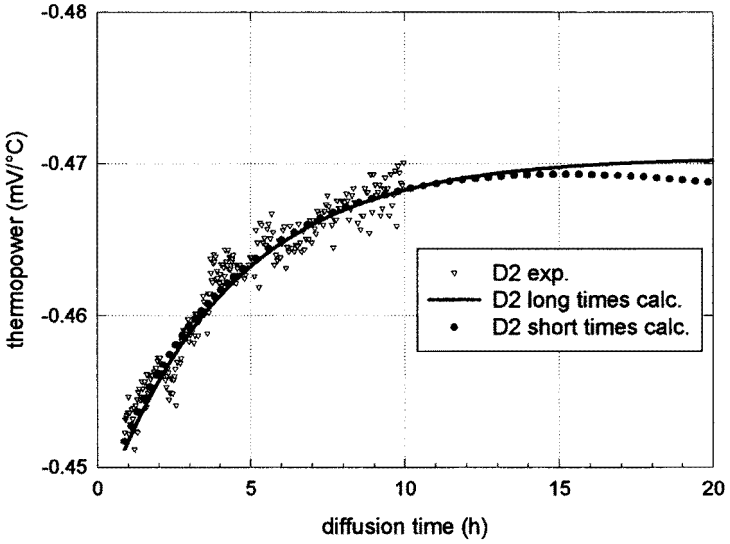

Figure 8. Thermopower results with time for D2 between 1 and 10 h and calculated curves corresponding to two types of equation, one valid for short times, and one for long times.

at long times permitting the asymptotic variation characteristic of the steady state. Figure 8 and expressions (4) and (5) are evidence that the experimental results coming from D1 should be fitted with the short-times equation (4) while the D2 results must necessarily be fitted with the long-times equation (5) especially for times larger than 10 h of diffusion time.

As we have already mentioned, the D2 measurements were much troubled after a few hours of diffusion (figure 7). The reasons for the trouble are still under discussion, but we assume that they come from the large variations of a reference 'ambient' temperature during the flight (16–23 °C). These variations themselves are bound to the numerous activation and deactivation of experiments which are proceeded during the same period of time. For identical reasons, we also noted large vacuum variations during this experiment, certainly also inducing temperature variations.

For these reasons, we have fitted the D2 results with two curves (figure 7), which represent extreme values (lower value and upper value) for the calculated parameters. The lower curve accounts for the results between 1 and 10 h of diffusion, while the upper curve is calculated with the results from 1–5 h and 12–18 h. The results coming from the two calculations differ slightly except for the initial thermopower ε_0, and permit us to have an idea of the resulting uncertainty. The main results for D1 and D2 are summarized in table 4.

The calculated ε_0,which is the initial thermopower, is in perfect agreement with the value measured on Earth for the salt composition used (eutectic $AgI_{0.72}/KI_{0.28}$, -0.415 mV $^\circ C^{-1}$ [18]—almost constant with temperature over the whole liquid range). The negative value means that the hot end is negatively polarized. The interdiffusion coefficient D_{Ag^+/K^+} is deduced from expression (3), the diffusion length being 3 cm. Thus, its value is less than one sixth that deduced from the use of the quasi-Darken relation with the Earth measured self-diffusion coefficients.

In addition, the small magnitude of D_{Ag^+/K^+} (about 5×10^{-5} cm^2 s^{-1}) around the eutectic composition, obtained during both flights, might be surprising because it appears quite similar to the values obtained in the dilute range by several authors with different

Table 4. Thermopower results obtained from D1 and D2 (the discrepancy between various experiments gives an estimation of the uncertainties).

	Experiment		
Parameter	D1	D2 (lower values)	D2 (upper values)
ε_0 (mV °C^{-1})	−0.398	−0.443	−0.441
ε_∞ (mV °C^{-1})	−0.439	−0.471	−0.476
τ (h)	4.61	4.26	5.50
D_{Ag^+/K^+} (cm^2 s^{-1})	5.50×10^{-5}	5.95×10^{-5}	4.61×10^{-5}
S_T (K)$^{-1}$ (from extrapolated thermopower at infinite time)	$+1.01 \times 10^{-3}$	$+0.718 \times 10^{-3}$	$+0.897 \times 10^{-3}$
S_T (K)$^{-1}$ (from analysis after one time constant)	$+1.39 \times 10^{-3}$		

methods (see for example [21, Klemm p 592]), with which we completely agree [9]. An explanation might be that the D_{Ag^+/K^+} variation with composition is not so important as predicted figure 3, so the uncertainty bound to its determination is of major importance. Let us recall that D_{Ag^+/K^+} is obtained from the diffusion time constant. As we already discussed, the D1 determination lacks precision because of the insufficient duration of the experiment, and the D2 experiment was highly perturbed. In both cases, this can lead to a more than 20% uncertainty on D_{Ag^+/K^+} which could explain its surprising constantness over the concentration range.

The Soret coefficient S_T is given by:

$$(\varepsilon_\infty - \varepsilon_0) = -RT/Ft_{K^+}S_T(1+\Gamma) \tag{6}$$

where Γ is the thermodynamic factor, t_{K^+} is the potassium transport number, and R, T and F are respectively the perfect-gas constant, the absolute temperature and the Faraday electric charge. As the thermopower is negative, $(\varepsilon_\infty - \varepsilon_0)$ is also negative, corresponding to a positive Soret in which the heavy component migrates towards the cold end of the cell. The D1 and D2 calculated values are given in table 4.

5.4. Sample analysis

The D1 samples were analysed after rapid cooling and return to Earth. The chemical analysis was performed on 2 mm thick slices perpendicular to the temperature gradient direction. The results given in figure 9 show the excellent linearity of the concentration variation along the sample for both experiments around the initial and mean value of 72% AgI. The linear variation along the cell (0.021 mol cm^{-1}) confirms that the thermodiffusion tends to enrich the cold side of the cell in silver and consequently to enrich the hot side of the cell in potassium. This fact was unknown before the experiment. The Soret coefficient S_T is then deduced from these values and from the formula:

$$S_T = \frac{1}{x_1 x_2}\frac{\operatorname{grad} x_1}{\operatorname{grad} T} \tag{7}$$

where $x_1 = 0.72$ mol%, $x_2 = 0.28$ mol%, $\operatorname{grad} x = 0.021$ mol cm^{-1} and $\operatorname{grad} T = 75\,^\circ$C cm^{-1}. This gives $S_T = +1.39 \times 10^{-3}$ K^{-1}; which is not far from the value calculated

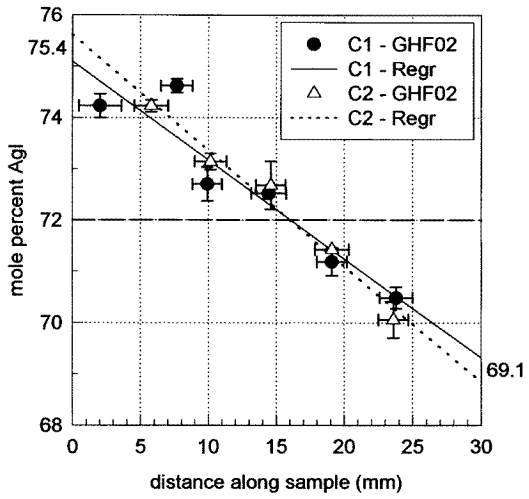

Figure 9. Analysis of the D1 samples along the temperature gradient axis.

from thermopower measurements (table 4). However, one point might ask a question. Taking account for the D1 duration (about one time constant), we can consider that this corresponds (as for a perfect exponential function) to 63% of the expected total variation (until infinite time). So, if the duration was sufficient, the Soret coefficient that we should have obtained should probably be multiplied by about 1.5, leading to a more probable value of around $+2 \times 10^{-3}$ K^{-1}. In those conditions, S_T obtained from the analysis is about twice that obtained from the thermopower variation. This difference can be explained by the insufficient cooling rate of the sample in spite of a helium injection in the furnace. In those conditions, the displacement of the solidification front along the sample during the 15 min necessary to obtain the solid material, tended to enrich the sample in the same conditions as the Soret effect.

5.5. Comparison D1-D2

The D2 results are of considerable interest and confirm the D1 values for a much longer experiment time, with respect to the time constant of the diffusion process. However, one should note that the D1 results we give come from the second D1 run which was performed at the end of the flight when all other experiments were over. They are then much more reliable because no perturbation occured during the experiment. The problem comes from the insufficient duration of this experiment which makes it difficult to calculate the parameters involved in the diffusion process if one takes into account for the slight discrepancies of the measurements. In contrast, the D2 duration was good but unfortunately, large thermal perturbations occurred during this experiment, which led to low precision in the experimental results. So it is difficult to give a valuable interpretation of the difference between the S_T values coming from the two experiments (table 4). One possibility is to attribute it to the difference in the composition of the melts (table 2); the other possibility is simply to consider the S_T differences as an uncertainty coming from the discrepancies in the experimental results

6. Conclusion

In conclusion, we have shown that a thermal diffusion process occurs in a molten salts mixture in space. Because this effect is small and is combined with perturbations from convective instabilities, few reliable experiments have been performed on Earth [1, 20]. We have demonstrated that microgravity *in situ* measurement of the Soret effect is possible with a better accuracy than from preceding experiments on Earth. The Soret coefficient is positive, corresponding to the heaviest component migrating towards the cold end of the cell. Although its value is small, around 1×10^{-3} K^{-1} (with an uncertainty of about 20%), it is open to measurement by two different methods (thermopower as a function of time and analysis of final composition, if the quenching can be sufficiently rapid to avoid the segregation). This is possible because the properties of the investigated fluid make it possible to analyse the time dependence of the process, providing a better basis for analysis. In addition, the analysis of the time variation of these properties will allow close analysis of the role of instabilities in space relative to those encountered under gravity.

Nevertheless, our experiment does not really show the shape of the concentration gradient induced by the applied thermal field (figure 6). In addition, we do not know whether convective instabilities (due to the residual 10^{-3}–$10^{-4} g_0$ acceleration) are present or not. *In situ* visualization of the sample is necessary, so an optical method (interferometric holography) of determining the exact experimental conditions of the process is under consideration as is the development of more precise measurements as a function of time for long-duration experiments. Our programme now takes this line, combining Earth experiments on a chosen viscous mixture and space experiments (*in situ* electrical and optical measurements) with additional studies among which are a study of the influence of the Prandtl number on the instability, and the influence of surface conditions.

Acknowledgments

This work on space experiments was supported by the French space agency. We are also indebted to the CNES staff, and more particularly to Hélène Benhaim and Daniel Buso for their help during the D2 flight preparation and also during the flight itself.

References

[1] Chanu J 1994 *Entropie* **184/185** 7
[2] Vogelsang R, Hoheisel C, Paolini G V and Ciccotti G 1988 *Phys. Rev.* A **38** 6296
[3] Rousseau B, Fuchs A H and Simon J-M 1994 *Entropie* **184/185** 62
[4] Tyrrell H J V 1961 *Diffusion and Heat Flow in Liquids* (London: Butterworths)
[5] Janz G J 1967 *Molten Salts Handbook* (New York: Academic)
[6] Claudy P, Letoffe J M, Fornazero J, Jal J-F, Bert J and Dupuy-Philon J to be published
[7] Levin E P, Robbins C R and McMurdie H P 1964 Phase diagrams for ceramists *Am. Ceramic Soc.* p 448
[8] Sternberg S, Adorian I and Galasice I 1966 *Electrochim. Acta* **11** 385
[9] Mellon H 1979 *Thesis* Lyon
[10] Anderson J S and Saddington K 1949 *J. Chem. Soc.* p 381
[11] Bert J, Henry D, Layani P, Chuzeville G, Dupuy J and Roux B 1984 *Proc. 5th European Symposium Material Sciences under Microgravity (Schloss Elmau, 5–7 November)* ESA SP 222
[12] Bert J and Dupuy J 1986 *Natur Wissenschaften* **73** 366
[13] Bert J, Moussa I, Henry D and Dupuy J 1986 *D1 Spacelab Scientific Mission, Proceedings II, Nordeney Symposium, 27–29th August* ed P R Sahm, R Jansen and M H Keller
[14] Bert J, Moussa I and Dupuy J 1986 *Proc. 6th European Symposium on Material Sciences under Microgravity Conditions (Bordeaux, 2–5 December)* ESA SP 256

[15] Moussa I 1989 *Thesis* Lyon
[16] Henry D 1986 *Thesis* Lyon
[17] Sundheim B R and Kellner J D 1965 *J. Phys. Chem.* **69** 1205
[18] Pezzati E, Schiraldi A and Magistris A 1973 *Z. Naturforsch.* a **28a** 1334
[19] Bert J and Dupuy-Philon J 1995 *D2 Spacelab Scientific Mission, Proceedings, Nordeney Symposium, Germany, 14–16 March 1994* ed P R Sahm, R Jansen and M H Keller pp 295–303
[20] Backlund V, Dupuy J, Gustafsson S and Lundén A 1967 *Z. Naturforsch.* a **22** 471
[21] Blander M 1964 *Molten Salt Chemistry* (New York: Wiley–Interscience)